Stability analysis of a red bed slope reservoir bank considering water–rock interaction characteristics

Hao Zhang[a,b], Zaiqiang Hu[a,*], Bin Ma[a], Xingzhou Chen[c]

[a]*School of Civil Engineering and Architecture, Xi'an University of Technology, Xi'an 710048, China,*
email: zh22001@126.com (H. Zhang)

[b]*Power China Northwest Engineering Co., Ltd., Xi'an 710065, China*

[c]*Xi'an University of Science and Technology, Xi'an 710054, China*

ABSTRACT

Changes in reservoir water level alter the hydraulic environment of bank slopes and negatively impact their stability by accelerating the process of water–rock interaction. This study, therefore, studied the failure characteristics of a red bed slope near the bank of a hydropower reservoir in Southwest China. Bank material specimens with various initial fracture angles were numerically simulated under different pore water pressure environments and a slope stability analysis was conducted to determine the resulting slope deformation characteristics and stability. The results show that: (1) Pore water pressure mainly affected the peak compressive stress and post-peak behavior of the rock. Under the same pore water pressure, the peak stress first increased and then decreased with increasing initial fracture angle. (2) The initial fracture angle mainly affected the distribution of microscopic tensile failures in the specimen, which in turn affected its compressive strength. The main factor controlling factor rock mass deformation and failure was the pore water pressure. (3) When the long-term water level fell to a given level, the safety factor of the bank slope was lower than that when the long-term water level rose to the same level. The main failure mode of the slope was a shear failure, while tensile failure exhibited a strong correlation with the safety factor. (4) The bank slope risked local instability when the long-term water level rose and risked sectional instability when the long-term water level fell, and there was instability and penetration of the section, indicating the possibility of landslides. (5) When the long-term water level fell, there was a considerable difference between the deformation of the shallow rock mass and the deformation of the deep rock mass, and the traction and deformation effect of the shallow rock mass on the deep rock mass was more obvious.

Keywords: Slope near the bank of a hydropower reservoir; Red bed slope; Water–rock interaction; Numerical simulation; Stability analysis

1. Introduction

With the gradual improvement and increasing, complexity of infrastructure projects related to water conservancy, hydropower, and transportation, the safe construction, operation, and maintenance of these projects will inevitably face challenges associated with geological conditions. Notably, the construction of dams associated with water conservancy and hydropower projects changes the environment,

and excavation during dam construction can expand the original joints and fractures in the underlying rock mass. During the water–rock interaction process along the shores of dam-created reservoirs, the structure as well as the physical and mechanical properties of the bank slope rock mass can deteriorate, causing the water–rock interaction process to further accelerate, decreasing the shear resistance and tensile strength of the sliding rock mass at the lower part of the bank slope. This leads to a gradual loss of slope stability

* Corresponding author.

and can induce local instability and failure that may in turn cause bank slope collapse, slippage, or other geological disasters. Indeed, there have been many large-scale landslides in the Three Gorges Reservoir area since the construction of the dam downstream, resulting in damage to roads and farmland and causing major economic losses [1–4].

Various research has already been conducted investigating the effects of reservoirs on their surrounding banks. Deng and Li [5] studied the mechanism by which the reservoir water level influences bank slope deformation and stability. Sahana et al. [6] established a model of rock mass strength degradation under the effects of water–rock interaction over time. Sufiyan et al. [7] studied the deformation and failure modes of different bank slope rock mass structure types. Zhang et al. [8] studied the stability change characteristics of bank slope fluid–solid coupling during sudden changes in water level. Chang et al. [9], Xu et al. [10], Li et al. [11], and Li [12] analyzed bank slope stability using numerical analysis.

Joints and fractures can have a significant impact on the physical and mechanical properties of rock, and their presence and distribution in a rock mass are therefore closely related to its failure and instability. As a result, a great deal of research has investigated the effects of joints and fractures on rock failure behavior. Dong et al. [13] conducted uniaxial compression tests on granite with two non-parallel fractures. Wang et al. [14] conducted numerical experiments on red sandstone with intermittent double fractures under different confining pressures. Lee and Jeon [15] et al. studied the influence of closed and open double fractures on the failure mode of a series of rock specimens. Yang et al. [16] used the finite element method to study the fracture initiation, propagation, and penetration modes of prefabricated fractured rock mass samples. These studies demonstrated that water level fluctuations can change the chemical, physical, and mechanical properties (internal friction angle and cohesion) of a bank slope rock mass in such a way as to promote the expansion and development of joints and fractures. As these fractures develop, the structure and mechanical properties of the rock mass further deteriorate, adversely affecting the deformation and strength of the rock mass.

To investigate the effects of water–rock interaction on the stability of reservoir slopes, this study took a red bed slope near the bank of a reservoir in Southwest China as the research object. Numerical simulations of rock behavior were then conducted considering the geometric parameters and distribution of fractures under the action of pore pressure to determine their influence on the physical and mechanical properties of the rock. The degradation law of the mechanical properties of the rock was then combined with a numerical analysis of bank slope stability to comprehensively analyze the bank slope deformation. The results of this analysis are expected to provide a theoretical reference for the construction of mitigation measures in areas newly subjected to the action of repeated water level fluctuations, such as reservoir and port slopes.

2. Target slope overview

2.1. Slope structure characteristics

The micro-topography of the red bed slope near the bank of the target reservoir is relatively developed, and mainly consists of two small mountain ledges with adjacent steep ridges and gullies; the natural slope follows the water flow direction, turning from the NNW to the NW. The lithology is a tertiary red bed with monzonite underneath. The top of the bedrock gradually rises from the upstream to the downstream of the slope; the overall stability of the natural slope is good. The tertiary red bed strata in this part had a strike of NE 75°–85° and a dip angle of 10°–14° to the NW. There are mainly three groups of structural planes in the rock formation: one is near-upright in the NW direction, one is a steep dip in the NE direction, and the final is a gentle dip. Some of the structural planes in the NW direction cut through the underlying conglomerate rock layer. The tertiary red bed is strongly weathered with a thickness of 15–20 m, and the excavation of the slope is mainly controlled by the above three groups of fractures. Under the repeated, alternating effects of the dry and wet environment associated with reservoir water storage and flood discharge, the rock mass structure of this Tertiary red bed has been continuously damaged and disturbed on both micro and macro levels, and as a result, the strength of the rock mass has been rapidly reduced as is shown in Fig. 1.

2.2. Analysis of instability mode

The Tertiary red beds considered in this study are very thick and exert the main control effect on the bank slope

Fig. 1. The original landform of the red bed slope is considered in this study.

stability; the inter-layer contact zone between the red bed and the underlying monzonite is an unconformity surface filled with clastic materials, and gradually rises from upstream to downstream following the direction of water flow. This zone readily becomes a weak structural surface under the action of the reservoir water, potentially leading to the failure of the upper Cenozoic Reservoir Bank. The red bed slope stability control conditions consist of a reservoir upper limit water level of 3,330.0 m and a reservoir low water level of 3,185.0 m when emptied under special circumstances. Existing geological survey data show that there is no specific structural surface on the rear edge of the red bed slope; the basic failure mode is the sliding of the red bed slope inter-layer contact zone and the shallow surface layer downward along the slope in a circular arc.

3. Numerical simulations

3.1. Numerical model and calculation process

In this study, the FLAC³D software was used to numerically simulate the compressive behavior of a red bed slope material specimen model under seepage pressure. As shown in Fig. 2, the model was 100 mm × 50 mm and comprised a total of 40,000 elements. Using the Mohr–Coulomb plastic model, specimen models with an initial fracture length and width of 10 and 3 mm, respectively, and different fracture angles of 0°, 45°, 90°, and 135° were subjected to compressive load under various seepage pressures of 0.6, 1.2, and 1.8 MPa, based on the actual situation of the target slope. The uniaxial compressive strength of a complete specimen collected for the site was determined by laboratory testing to be 23.5 MPa, and the value obtained from the complete rock numerical simulation

with no fractures or pore water pressure was 22.7 MPa. The shear strain increment cloud image obtained by the simulation was similar to an image of the fracture captured during the laboratory compression test, as shown in Fig. 3 along with the stress–strain relationship.

The specific process entailed by the numerical water–rock coupling simulation is to apply water pressure at the bottom face of the specimen with the upper face serving as the water outlet and the lateral surface of the specimen sealed by an impervious boundary. The seepage pressure is defined as the difference between the upstream and downstream
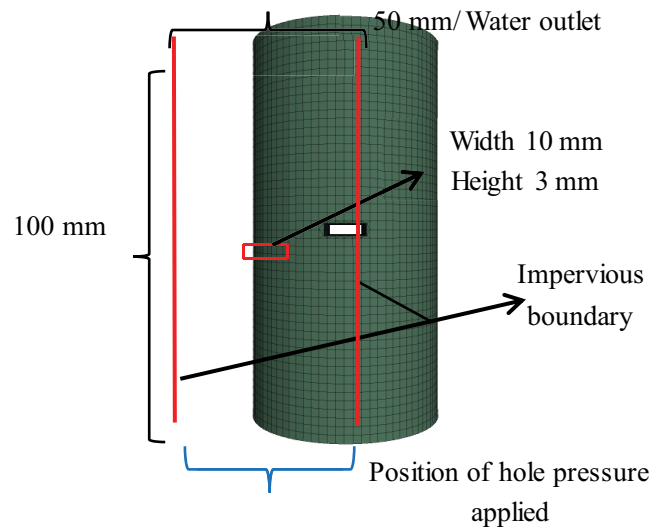
Fig. 2. Numerical simulation model.
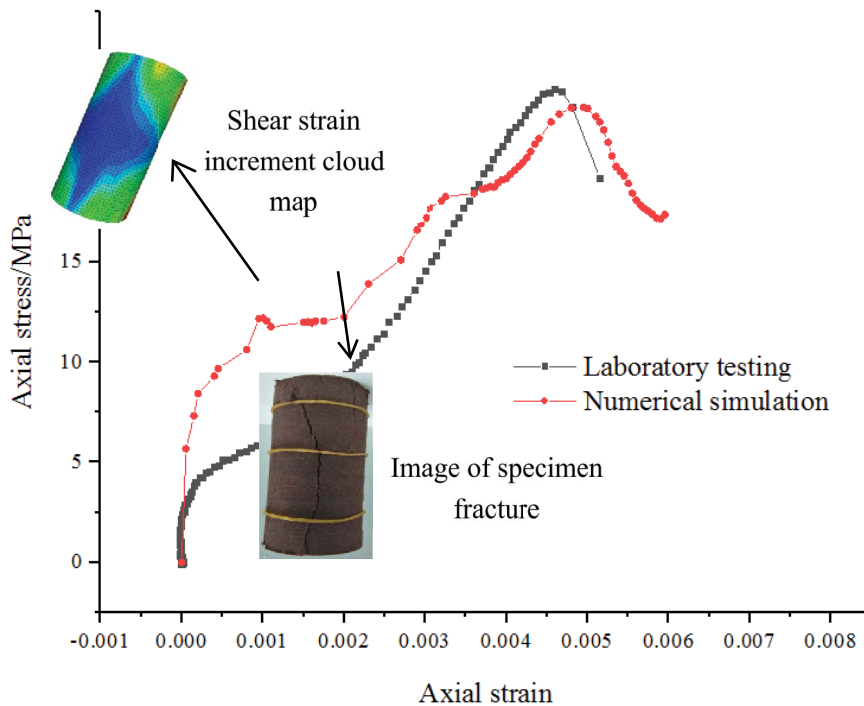
Fig. 3. Stress–strain curves of the simulated and actual specimens under uniaxial compression.

water pressure, and is used to simulate the effects of pore pressure in this study. Note that in the process of applying seepage pressure, the mechanical process is closed, which indeed maintains a constant pore pressure consistent with the reality of the subject red bed slope, but also prevents the transient response of the pore pressure, potentially affecting the accuracy of the numerical simulation results.

3.2. Stress–strain relationship

The simulated compressive stress–strain curve of the specimen without seepage pressure is shown for different initial fracture angles in Fig. 4, in which it can be seen that the compressive stress decreased rapidly after reaching its peak, indicating obvious brittle characteristics. The peak stress increased with the initial fracture angle; the peak stress for the horizontal fracture was clearly the smallest. It is speculated that the reason for this relationship may be that the horizontal projection of a more horizontal fracture is larger during specimen compression, and as the external force does work on the specimen, the energy accumulated in the specimen is released over time along this horizontal projection; thus, the maximum stress peak was observed when the fracture angle was vertical. When the fracture angle exceeded 90°, the peak strength decreased; the stress–strain curves for 135° and 45° fracture angles were quite similar. Indeed, the numerical simulations yielded an axisymmetric graph, in which the elastic moduli of specimens with different fracture angles (as determined by the slopes of their stress–strain curves) were basically the same on either side of 90°.

The compressive stress–strain curves of the simulated rock specimens subjected to various seepage pressures under different initial fracture angles are shown in Fig. 5, in which it can be seen that under all three seepage pressures, the curves for the same initial fracture angle remained

close before the compressive peak stress, and the peak compressive stress when no initial fracture was present was obviously higher than that when an initial fracture was present. However, the peak compressive stress decreased more obviously under higher seepage pressures before remaining relatively flat. This is obviously different from the case in which no seepage pressure was present, indicating that pore water pressure mainly affected the peak compressive stress value and post-peak behavior of the rock. Furthermore, under a given seepage pressure, as the initial fracture angle increased, the peak compressive stress first increased and then decreased, which is consistent with the observed change law in the case with no applied seepage pressure.

3.3. Law of strength deterioration

The compressive strengths obtained according to Fig. 5 are shown in Fig. 6, in which it can be observed that the compressive strength gradually decreased with increasing seepage pressure. In view of the small value of seepage pressure in the early stage, the magnitude of decrease was not immediately obvious; however, as the seepage pressure increased, the decrease in compressive strength gradually became more prominent. For example, the uniaxial compressive strength was determined to be 22.2 MPa for the specimen with a 90° initial fracture under no seepage pressure, but decreased to 20.1 MPa for the same specimen under a seepage pressure of 1.8 MPa; a decrease of nearly 10%. This decrease occurred because the cement between the mineral particles, which was originally monolithic, developed expanding fractures under the action of the strong pore pressure; these fractures joined and merged, changing the specimen's structure from its initial compact state into a more porous structure. In addition, when the applied seepage pressure was the same, the compressive strengths of the specimens without initial fractures were
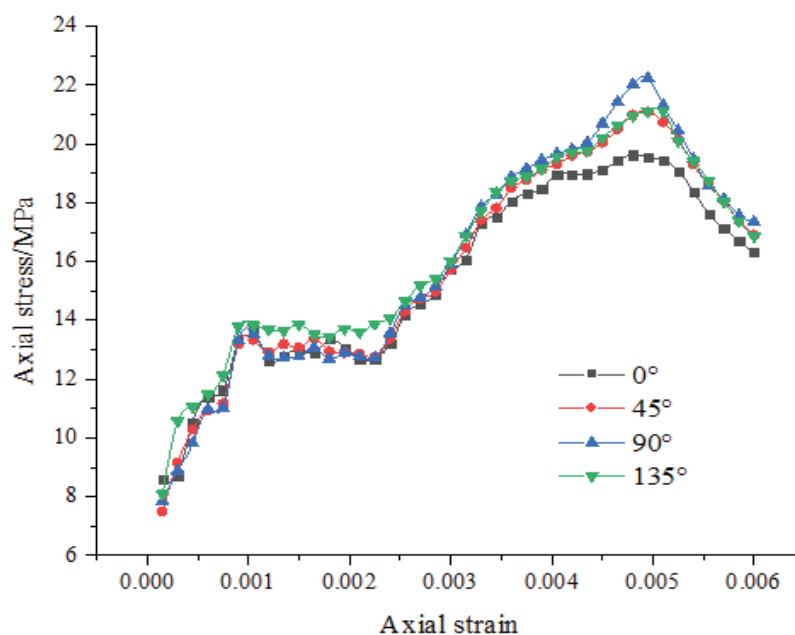
Fig. 4. Compressive stress–strain curves of specimens with different initial fracture angles under no seepage pressure.
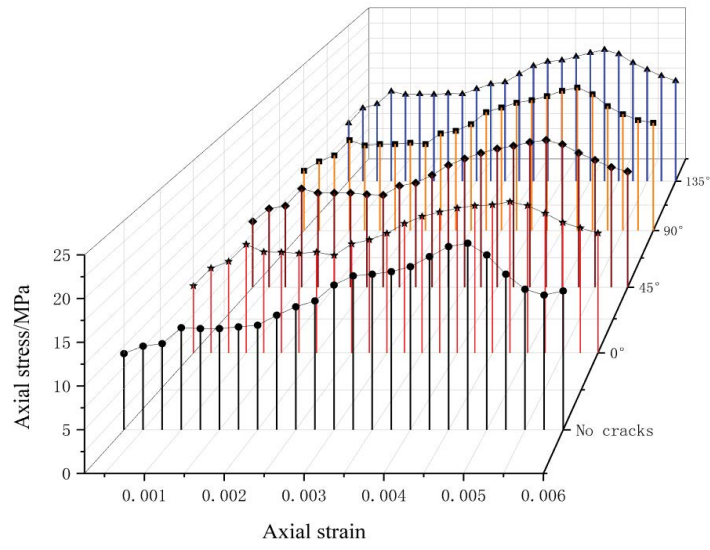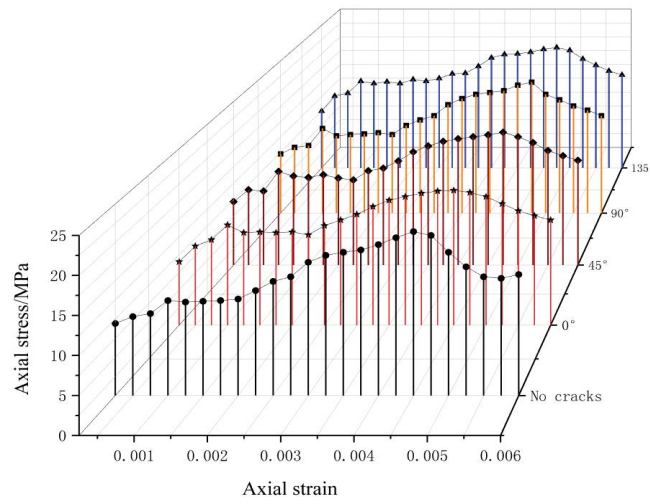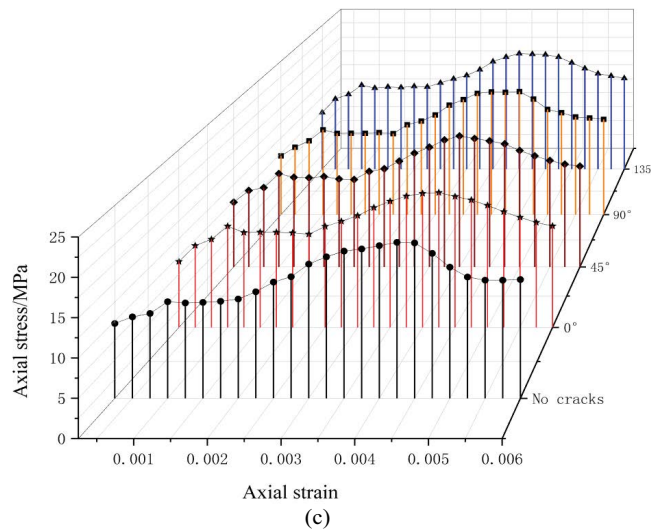
Fig. 5. Compressive stress–strain curves for different fracture angles under different seepage pressures: (a) Seepage pressure = 0.6 MPa, (b) Seepage pressure = 1.2 MPa and (c) Seepage pressure = 1.8 MPa.
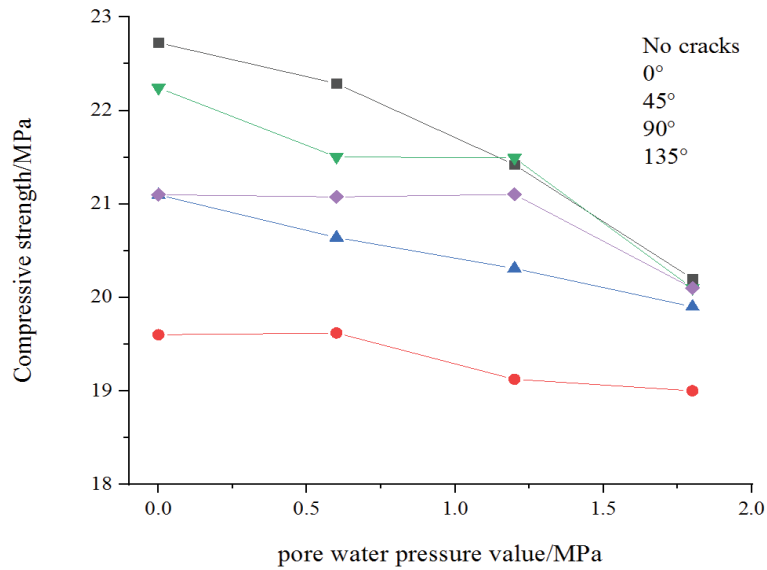
Fig. 6. Compressive strength according to initial fracture angle and seepage pressure.

greater than those of the specimens with initial fractures, and first increased before decreasing with increasing initial fracture angle. For example, the compressive strength of the specimen with a horizontal initial fracture under a seepage pressure of 0.6 MPa was 19.6 MPa, whereas that of the specimen with a 90° initial fracture angle under the same seepage pressure was 21.5 MPa. Furthermore, the difference between the maximum and minimum compressive strengths according to initial fracture angle gradually decreased with increasing seepage pressure because the mineral particle skeleton softened, while the increase in internal cracks and fractures gradually slowed due to the waning influence of the fracture angle at the higher pore water pressures that accompany larger seepage pressures. When a fractured rock mass is subjected to a water-bearing geological environment, special attention should therefore be paid to the seepage pressure as the main controlling factor that causes rock mass deformation and failure under high seepage pressure is the pore water pressure, and there is little relationship with the stress fracture angle.

3.4. Failure characteristics

The plastic region and maximum shear strain increment cloud map obtained from the numerical simulations of red bed rock specimens containing different initial fracture angles and subjected to different seepage pressures were used to study the distribution of failure regions. The analysis results show that the failure types of the specimens were roughly the same. Therefore, the failure characteristics of the specimens subjected to a seepage pressure of 1.2 MPa, shown in Table 1, were analyzed and are presented in this paper as representative. The FISH language included in FLAC[3D] was used to obtain the volume of elements corresponding to the type of failure, as shown in Fig. 7.

It can be seen from Table 1 that the specimens mainly displayed "X"-shaped failure characteristics. Tension–shear failures occurred near the fracture shoulder angle,

Table 1
Failure types of fractured specimens under a seepage pressure of 1.2 MPa

Crack angle	0°	45°	90°	135°
Plastic zone distribution				
Maximum shear strain increment				

the cracking perpendicular to the upper and lower end faces indicated primarily tensile failures, and shear failure occurred in large areas. Thus, the specimen failure began at the shoulder, then expanded along the loading direction, but did not penetrate the specimen. Then, tensile failure occurred at the upper and lower ends of the specimens, and obvious shear failure zones were formed. The maximum shear strain increment cloud map distribution for the 90° initial fracture specimen was relatively uniform, indicating that there was no obvious stress concentration phenomenon for this specimen. Both the maximum shear strain increment cloud map and the distribution of the failure area of the 0° initial fracture specimen were more uneven and larger than those of the other specimens, reflecting

the lower compressive strength of this specimen. It can be seen from Fig. 7 that the specimens mainly failed in shear; indeed, the volume of elements failing in tension was about 1/4 to 1/3 that of those failing in shear. The volume and quantity of elements failing in tension first increased and then decreased with increasing initial fracture angle, following a change law similar that observed for the compressive strength. However, the volume and quantity of elements failing in shear first decreased, then increased with increasing initial fracture angle. This indicated that the initial fracture angle mainly influenced the compressive strength of the specimen through the distribution and quantity of microscopic tensile failures.

4. Slope stability analysis

4.1. Calculation method and modeling

Due to its limitations, FLAC[3D] cannot truly realize an unsaturated seepage analysis, so there are certain limitations in it application to analyze the rise and fall of the reservoir water level. The FLAC[3D] software adopts the following equation to describe the saturated–unsaturated seepage in a porous continuous media:

$$q_i = -k_r(S)K_{ij}h, j = -k_r(S)K_{ij}(\Psi + z), j \tag{1}$$

where q_i is the unit flow vector; K_{ij} is the permeability coefficient tensor; $k_r = s^2(3-2s)$ is the relative permeability coefficient, in which s is the saturation; $\Psi = p/\gamma_w$, in which p is the pore water pressure and γ_w is the weight of water; and z is the position head.

It can be seen from the equation above that the key problem of the saturated–unsaturated seepage equation lies in the relationship between the permeability coefficient and the saturation, but the FLAC[3D] calculation process defaults to the condition in which the bank slope rock mass is fully saturated; that is, the saturation is 1.0. As the reservoir water cannot infiltrate through the head boundary above the

saturation line, the saturated–unsaturated seepage equation becomes meaningless. In this study, by referring to the research of Shen et al. and Reyes et al. [17,18], the saturation of the water pressure boundary element and node was set to 1.0, the fluid tensile strength was set to 0, the negative pressure mechanism was closed, the saturation of the elements below the saturation line was set to 1.0, and the saturation of the elements above the saturation line was set to 0. In the process of realizing this calculation, as the internal saturation of the slope changed, the calculation domain for seepage was expanded inward, representing the gradual infiltration of reservoir water into the deeper parts of the slope. Normal displacement constraints were imposed on the side boundary of the model, and displacement constraints were imposed on the bottom boundary. The resulting slope was a free boundary surface, shown in the numerical calculation model in Fig. 8, consisting of 36,387 elements and 34,099 nodes in total.

4.2. Safety factor

The traditional Mohr–Coulomb strength criterion takes the shear of rock and soil as the physical failure mechanism. In the calculation process, the factor F^{trail} was selected to reduce the shear capacity determined according to the relevant equation until the slope experienced instability and failure. The value of F^{trail} at failure was then considered to be the slope safety factor. However, rock–soil mass materials may experience tensile failure in certain stress environments, but this failure equation can only express the shear failure of the rock and soil material of the slope. Therefore, for the rock–soil slopes in this study, the change in the tensile strength of the rock–soil mass was considered during the reduction calculation process according to previous suggestions [19] as follows:

$$c^{trail} = \frac{c}{F^{trail}} \tag{2}$$
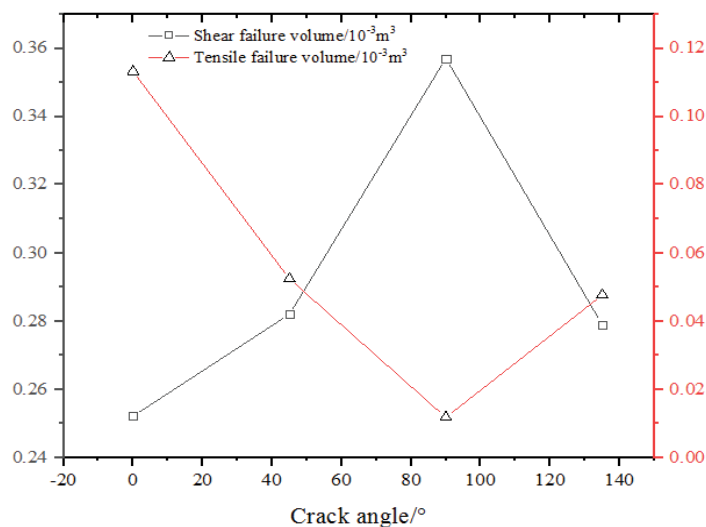
Fig. 7. Tensile and shear failure volumes of fractured specimens under a seepage pressure of 1.2 MPa.

$$\varphi = \arctan\left(\frac{\tan\varphi}{F^{\text{trail}}}\right) \qquad (3)$$

where c^{trail} is reduced cohesion of rock–soil and c is cohesion of rock–soil. The scheme applied for the numerical calculation of failure and the corresponding safety factors are shown in Table 2.

The safety factor against failure gradually decreased when the water level increased above the long-term level because the accompanying increase in pore water pressure caused the shear strength of the rock mass to decrease rapidly. However, a decrease from the long-term water level to the same elevation had a larger impact on the safety factor. For example, the safety factor of the slope was 2.11 when the long-term water level rose to 3185.0 m, but was 1.68 when the long-term water level fell to 3185.0 m. This is because the excess pore water pressure was not dissipated in time as the water level fell, increasing the excess pore water pressure at the exterior of the slope. Furthermore, the mechanical parameters of the rock mass had deteriorated under immersion, reducing the safety factor of the slope. As the long-term water level increased, the safety factor increased. For example, the slope safety factor was 1.04 when the long-term water level fell to 3,330.0 m, but was 1.40 when the long-term water level rose to 3,330.0 m. This is because the rise in water level was equivalent to an increase in the compressive constraints applied to the slope, which is conducive to its safety and stability. Therefore, during the rapid rise of reservoir water level, the surrounding slopes will remain stable, and slope instability is likely to occur when the reservoir water level falls rapidly and by large amounts. Furthermore, during the ongoing process of water level fluctuation, the immersed and eroded rock mass is gradually damaged, and the water–rock physical and chemical interactions are repeated, intensifying the development of rock mass fractures and decreasing the strength of the rock mass. As the water level continues to fluctuate repeatedly, the rate of fracture development gradually decreases and eventually becomes steady [20].

4.3. Maximum shear strain increment

The shear strain model evaluated in this study adopted the Mohr–Coulomb strength theory. The location at which the shear strain increment in a rock mass is largest is the most prone to deformation and failure. Therefore, the maximum shear strain increment can be used as a basis for the analysis of rock mass stability. Cloud maps of the maximum shear strain increment of six schemes were therefore output (the area with the largest shear strain is indicated in red) to compare the slope stability under different working conditions. On the whole, the slope stability was found to be quite good, and there was no overall instability, but the sectional and local shear strain increments were large, indicating sectional and local instability, and thereby potentially unstable rock masses [21].

Comparing schemes 2, 4, and 5 shown in Fig. 9, it can be observed that as the long-term water level rose, the failure area gradually deepened, the strain gradually increased,
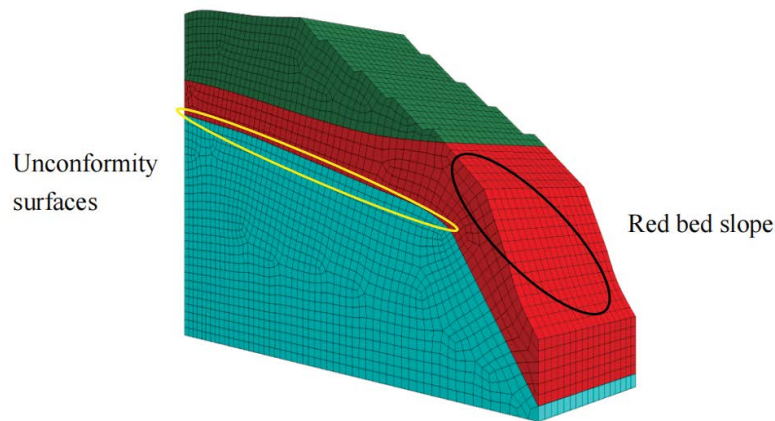
Fig. 8. Numerical simulation of slope seepage.

Table 2
Scheme for numerical calculation of failure and corresponding safety factors

Scheme	Water (m)	Safety factor	Scheme	Water (m)	Safety factor
Scheme1	/	2.14	Scheme2	3185.0 m	2.11
Scheme3	3,185.0 m drawdown	1.68	Scheme4	3,240.0 m impounded level	1.69
Scheme5	3,330.0 m	1.03	Scheme6	3,330.0 m water-level rise	1.40

and there was a gradual increase in penetration. As the long-term water level fell, the shear strain value increased more obviously, as did its range, reaching deeper than when the long-term water level rose, and the stability decreased more rapidly. Multiple potentially unstable regions were observed near the elevations of 3,210 and 3,260 m, where sectional instability was likely due to the influence of the water pressure change over the water level cycle. This accelerates the water–rock interaction process, gradually increasing the shear strain increment. The decrease in reservoir water level accelerates the deterioration of the physical and chemical properties of the rock mass, dissolving its internal cementing materials, weaking the particle bonding ability within, and gradually increasing its porosity. This further promotes the erosion of the rock mass, deepening the macroscopic failure area. In addition, the decrease in water level had a more obvious influence on the distribution of the shear strain increment, as indicated by the unloading of stress in the bank slope rock mass. This causes the mechanical parameters of the rock mass to deteriorate, the shear strain increment to increase, and the stability to decrease to less than that in present when the water level rises [22].

4.4. Plastic zone

Using the FISH language for programming design included in the FLAC^{3D} software, statistics can be obtained classifying the quantity of plastic rock mass in the numerical model, as shown in Fig. 10.

It can be seen from the figure that, as a whole, the reservoir water level fluctuation presented a characteristic state with shear failure as the mainstay and tensile failure as a supplement. Fluctuations in the water level led to an increase in the number of elements failing in tension,
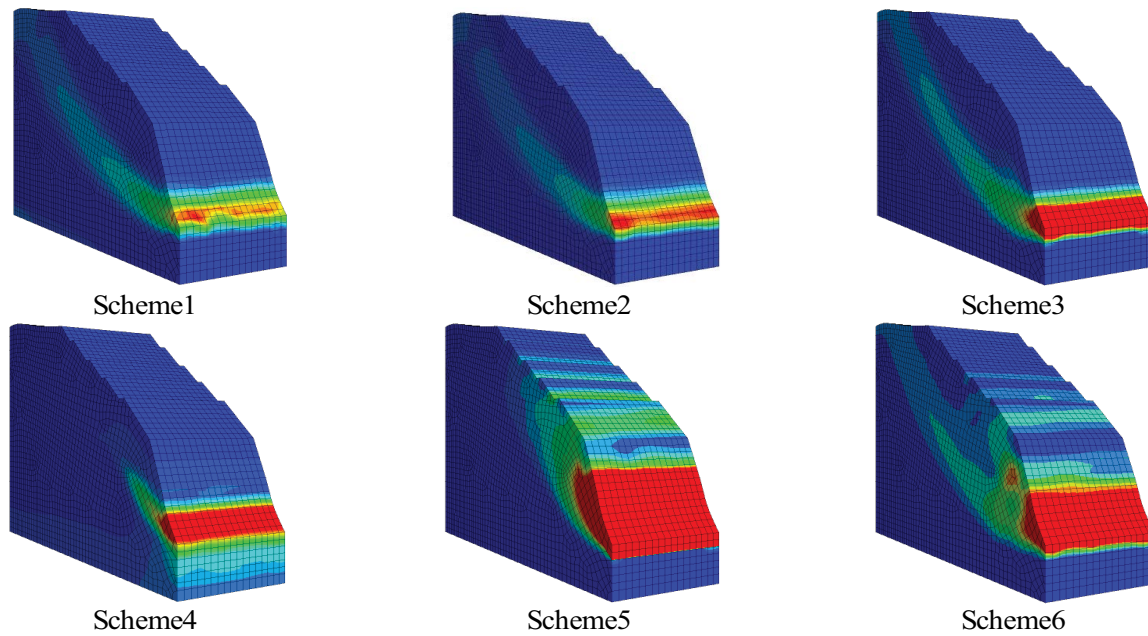
Fig. 9. Shear strain increment cloud map for six schemes.
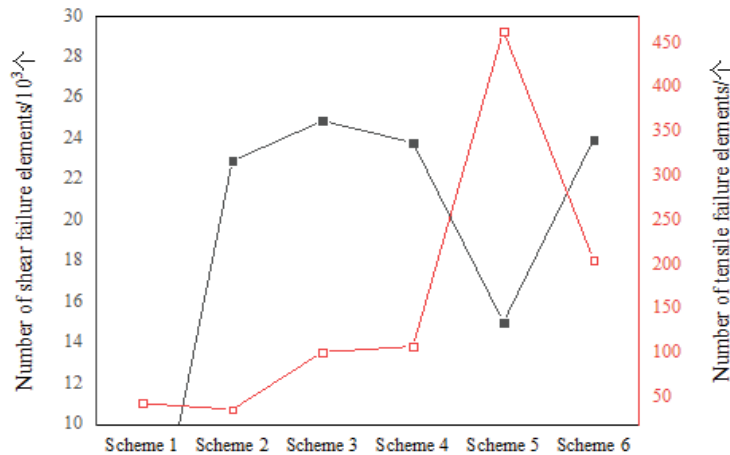
Fig. 10. A number of units with failure.
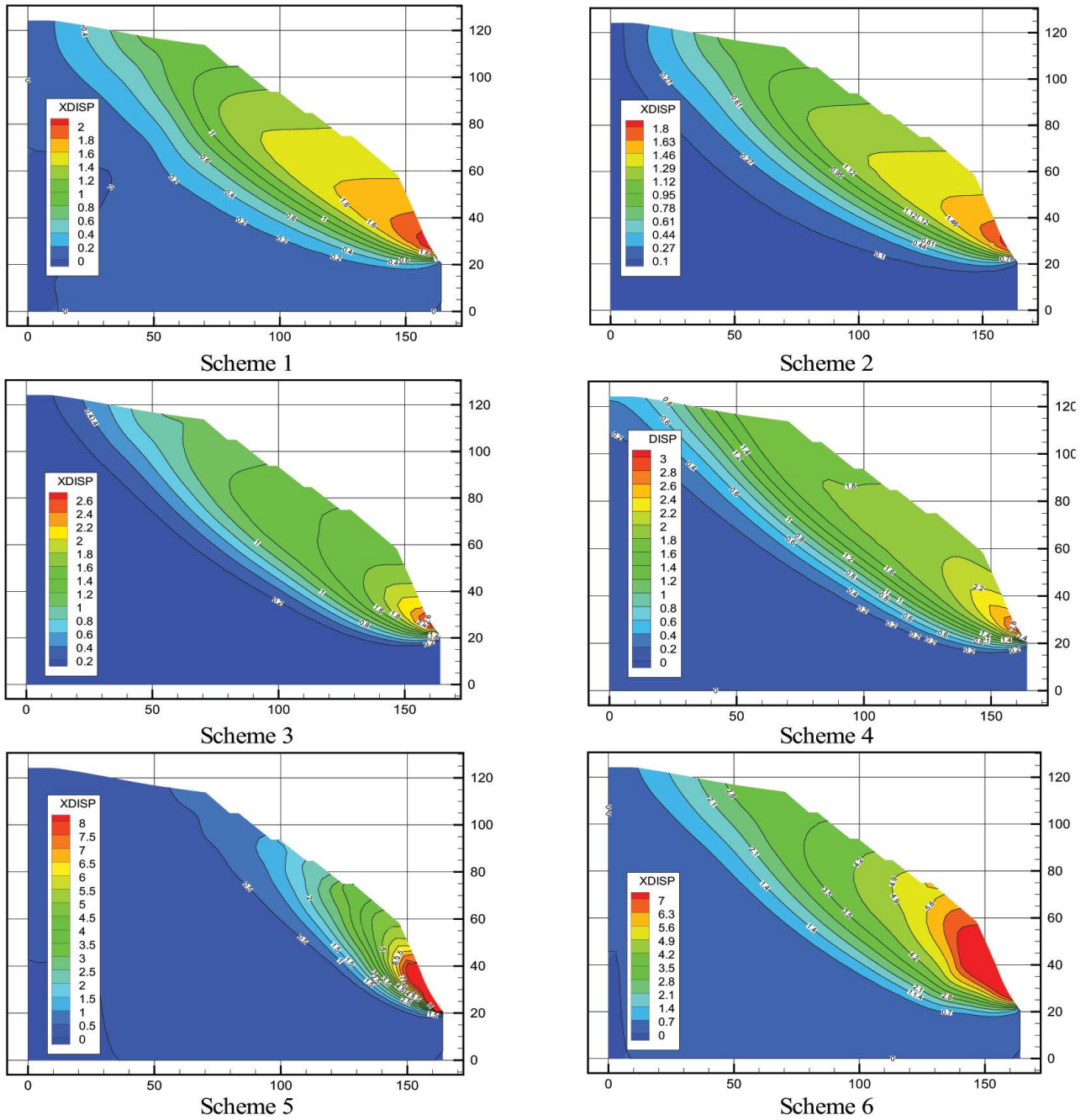
Fig. 11. Horizontal displacement cloud map of the inside of the rock mass (units in cm).

and for the same water level, a falling water level caused significantly more elements to fail in tension failure than a rising water level. Thus, it can be observed that the stability of the bank slope was considerably reduced when the water level fell, indicating that accidents such as landslides are more likely to occur; this is basically consistent with the actual situation around the target reservoir.

When a reservoir is filling, the pore water pressure in the surrounding banks increases, causing a change in the stress environment of the rock mass. In addition, there are a large number of micro-cracks, fractures, joints, etc.,

inside the rock mass, resulting in the acceleration of the water–rock deterioration process and forming a favorable physical, chemical, and infiltration environment for the development and expansion of cracks and fractures. This in turn results in a more rapid deterioration of the shear strength of the submerged rock mass. Thus, the deformation and failure of the slope is mainly dominated by shear failure. However, comparing the changes in the volume of elements failing in tension or shear, it was found that the volume of elements failing in shear was weakly correlated with the safety factor, whereas the volume of units failing

in tension was strongly correlated with the safety factor, despite the fact that the latter comprised fewer elements. Furthermore, about ten times more elements were observed to be failing in tension at a water level of 3,330.0 m than at a water level of 3,185.0 m. Thus, ensuring the tensile strength of the rock mass is the key factor for ensuring the safety and stability of the slope.

4.5. Displacement

To obtain the law describing the internal displacement of the rock mass as the reservoir water level rose and fell, a section was set in the middle of the simulation model to obtain a horizontal displacement cloud map inside the rock mass, as shown in Fig. 11. It can be observed in the figure that the horizontal displacement inside the rock mass presented an obvious step-like change, with the displacement gradually decreasing with distance into the rock mass. The change law of the horizontal displacement can be basically divided into an adjustment zone, a stable zone, and a protolith zone. The adjustment zone was located in the range of 0–25 m, where the horizontal displacement changed drastically. This displacement was small when the water level rose and large when the water level fell. The stable zone was located around 50 m into the rock mass, where the change in displacement was small regardless of water level change. Finally, the protolith zone near the bedrock exhibited significantly reduced displacement compared to the other zones.

Therefore, a rising water level can be considered equivalent to adding constraints to the bank slope rock mass. Furthermore, and the internal rock mass displacement change was relatively continuous, indicating good internal stability. However, when the water level fell, the internal displacement of the rock mass was discontinuous, indicating that large fractures are prone to occur within, reducing the stability of the rock mass. The horizontal displacement increment of the landslide body owing to the rise of the reservoir water level was very small overall, and was larger at the rear edge of the landslide mass than at of the front edge. On the other hand, the horizontal displacement increment of the landslide body owing to the falling reservoir water level was large, and the horizontal displacement increment of the landslide front edge was much larger than that of the rear edge; this will probably result in the instability and failure of the landslide mass. Therefore, the front edge of the landslide body near the reservoir bank is recognized as a key region that affects the stability of the slope. This region should accordingly be given strong consideration for slope treatment and monitoring.

5. Conclusion

This study conducted a series of numerical simulations of red bed slope behavior along the bank of a reservoir. The following conclusions were obtained from the results of the simulations.

• The pore water pressure, as induced in this study by seepage pressure, had a significant impact on the peak compressive stress and post-peak mechanical characteristics of the simulated red bed material specimen.

A horizontal initial fracture was found to have a more obvious impact on the peak compressive stress. As the initial fracture angle increased, the peak stress first increased and then decreased, while the compressive strength gradually decreased.

• The compressive strength of specimens with different initial fracture angles gradually tended to the same value and the degree of influence of the initial fracture angle on the specimens behavior gradually decreased with increasing seepage pressure. The specimens mainly presented "X" shaped failure characteristics, indicating mainly shear failure; the shoulder angle presented tensile–shear failure, and the upper and lower faces presented tensile failure.

• The fluctuations of the reservoir water level were observed to have a significant impact on the safety factor against slope failure. When the long-term water level fell to a given elevation, the bank slope safety factor was lower than that when the long-term water level rose to the same elevation, and the risk of slope instability increased when the reservoir water level fell rapidly.

• The bank slope exhibited a risk of local instability when the long-term water level rose, exhibited a risk of segmental instability when the long-term water level fell, and segmental instability and penetration were generally observed, indicating overall instability and the potential for landslides.

• The horizontal displacement was found to play a major role in the deformation and failure of the bank slope rock mass. When the long-term water level fell, the difference between the deformation of the shallow rock mass and the deformation of the deep rock mass was large, and the traction and deformation effect of the shallow rock mass on the deep rock mass was more obvious.

References

[1] J.L. Li, Unloading rock mass mechanics, China Water Power Press, Beijing, 2003, pp. 5–6.
[2] S. Wang, K. Zhang, L.P.H. van Beek, X. Tian, T.A. Bogaard, Physically-based landslide prediction over a large region: scaling low-resolution hydrological model results for high-resolution slope stability assessment, Environ. Modell. Software, 124 (2020) 104607, doi: 10.1016/j.envsoft.2019.104607.
[3] X.P. Zhou, Y.X. Zang, Unloading Rock Mass Constitutive Theory and Application, Science Press, Beijing, 2007.
[4] T.X. Wang, S.-R. Wu, J.S. Shi, P. Xin, L. Shi, A comparative study of typical engineering landslide disasters both in China and abroad, Geol. Bull. China, 32 (2013) 1881–1899.
[5] H.F. Deng, J.L. Li, Research on the influence mechanism of water level fluctuation on the bank landslide deformation and stability, J. Hydraul. Eng., (2014) 45–51.
[6] M. Sahana, S. Rehman, A.K. Paul, H. Sajjad, Assessing socio-economic vulnerability to climate change-induced disasters: evidence from Sundarban Biosphere Reserve, India, Geol. Ecol. Landscapes, 5 (2021) 40–52.
[7] I. Sufiyan, K.D. Mohammed, J.I. Magaji, Assessment of crop yield and rainfall simulation in Nasarawa Town Nasarawa State Nigeria, J. Clean WAS, 4 (2020) 75–78.
[8] J.-Y. Zhang, L.-P. Wan, H.-Y. Pan, J.-L. Li, Z.-S. Luo, H.-F. Deng, Long-term stability of bank slope considering characteristics of water-rock interaction, Chin. J. Geotech. Eng., 39 (2017) 1851–1858.
[9] Z.-H. Chang, F.Q. Wu, H.-Y. Liu, S.W. Qi, Bank slope types and rock mass structural features in new fengjie county, three gorges reservoir region, Chin. J. Rock Mech. Eng., 24 (2005) 3057–3063.

[10] W.-J. Xu, R.-L. Hu, Z.Q. Yue, R.-J. Tan, R.-J. Li, R.-Y. Zeng, Numerical simulation on stability of right bank slope of Longpan in Tiger-Leaping gorge area, Chin. J. Geotech. Eng., 28 (2006) 1996–2004.

[11] T. Li, N.-W. Xu, F. Dai, T.-B. Li, Y.-L. Fan, B. Li, Stability analysis of left bank abutment slope at Baihetan hydropower station subjected to excavation, Rock Soil Mech., 39 (2018) 665–674.

[12] H.Y. Li, Slope stability analysis of Longjiang River large bridge based on 3-D Fast Lagrangian Method (FLAC3D), J. Wuhan Univ. Technol., 32 (2010) 61–64.

[13] J.-Y. Dong, J.-H. Yang, W.-H. Sun, Z.-Q. Huang, D. Wang, G.-X. Yang, Prediction of deformation and failure of a large-scale deposit slope during reservoir water level fluctuation, Rock Soil Mech., 32 (2011) 1774–1780.

[14] L.F. Wang, L.G. Li, X. Yang, Instability initiation mechanism of gravel soil slope in Three Gorges Reservoir: case study of Hongyanzi landslide in Wushan County, Chin. J. Geotech. Eng., 40 (2018) 209–214.

[15] H.W. Lee, S.K. Jeon, An experimental and numerical study of fracture coalescence in pre-cracked specimens under uniaxial compression, Int. J. Solids Struct., 48 (2011) 979–999.

[16] S.Q. Yang, Y.H. Huang, S. Wen, Experimental study on mechanical properties of non-coplanar double fissure red sandstone after high temperature, Chin. J. Rock Mech. Eng., 34 (2015) 440–451.

[17] B.T. Shen, O. Stephansson, H.H. Einstein, B. Ghahreman, Coalescence of fractures under shear stresses in experiments, J. Geophys. Res., 100 (1995) 5975–5990.

[18] O. Reyes, H.H. Einstein, Failure Mechanisms of Fractured Rock – A Fracture Coalescence Model, Proceedings of 7th International Congress on Rock Mechanics, Aachen, Germany, 1991, pp. 333–340.

[19] Z.M. Jiang, X.H. Xiong, L. Zeng, Analysis of slope unsaturated rainfall infiltration based on FLAC~(3D) platform, Rock Soil Mech., 35 (2014) 855–861.

[20] Q.A. Wu, Study on Slope Stability of Hydropower Station Under Reservoir Water Level Fluctuation Condition, Dalian University of Technology, 2017.

[21] Z.J. Zhou, J.K. Chen, Z.Y. Wu, L. Pei, K. He, Failure criteria and the yield criterion in the numerical calculations of slope stability, Sichuan Daxue Xuebao (Gongcheng Kexue Ban)/J. Sichuan Univ. (Eng. Sci. Ed.), 46 (2014) 6–12.

[22] K. Zhang, S. Wang, H.J. Bao, X.M. Zhao, Characteristics and influencing factors of rainfall-induced landslide and debris flow hazards in Shaanxi Province, China, Nat. Hazards Earth Syst. Sci., 19 (2019) 93–105.